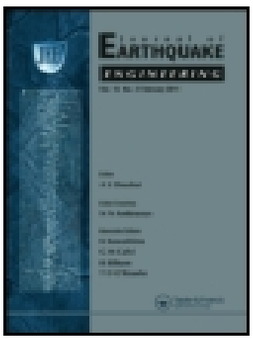

Journal of Earthquake Engineering

ISSN: 1363-2469 (Print) 1559-808X (Online) Journal homepage: http://www.tandfonline.com/loi/ueqe20

Effectiveness of Pile Reinforcement in Liquefied Ground

Duruo Huang, Gang Wang & Feng Jin

To cite this article: Duruo Huang, Gang Wang & Feng Jin (2018): Effectiveness of Pile Reinforcement in Liquefied Ground, Journal of Earthquake Engineering, DOI: 10.1080/13632469.2018.1456494

To link to this article: https://doi.org/10.1080/13632469.2018.1456494

Published online: 19 Apr 2018.

JOURNAL OF EARTHQUAKE ENGINEERING
https://doi.org/10.1080/13632469.2018.1456494

Taylor & Francis
Taylor & Francis Group

Effectiveness of Pile Reinforcement in Liquefied Ground

Duruo Huang[a], Gang Wang[b], and Feng Jin[a]

[a]Department of Hydraulic Engineering, Tsinghua University, Beijing, China; [b]Department of Civil and Environmental Engineering, Hong Kong University of Science and Technology, Clear Water Bay, Hong Kong, China

ABSTRACT

Installing reinforcement piles is an effective method to mitigate ground movement in liquefied soils. In this study, the effectiveness of the pile-reinforcement method is evaluated using an advanced finite element program OpenSeesPL. Parametric studies are conducted to investigate key parameters in the mitigation model, including pile area replacement ratio, pile diameters and pile-embedment length. The effectiveness of pile reinforcement to reduce large flow deformation in the liquefied ground is significantly influenced by the pile-embedment condition. It is recommended the embedment length is at least 1 m or 2 m if the underlying soil is a dense or a medium sand.

ARTICLE HISTORY
Received 17 May 2017
Accepted 20 March 2018

KEYWORDS
Liquefaction; Pile Reinforcement; Numerical Simulation; Embedment Length; Soil–Pile Interaction

1. Introduction

Earthquake-induced soil liquefaction has caused significant damage to buildings and foundations, due to excessive ground deformation and loss of strength in liquefied soils [Tokimatsu and Nomura, 1991; Ishihara, 1993; Berrill and Yasuda, 2002; Ye *et al.*, 2016; Ye and Wang, 2015, 2016]. Case histories learnt from major earthquakes in recent 50 years have led to many advances in developing ground improvement approaches to reduce the risk of liquefaction and associated ground deformation, including deep soil mixing, dynamic compaction, jet grouting, cementation, stone column, and pile-reinforcement methods [e.g., Adalier and Elgamal, 2004; Zhang and Wang, 2010; Nguyen *et al.*, 2013; Lew *et al.*, 2014; Rayamajhi *et al.*, 2014]. Among them, installation of reinforcement piles has been proved as an effective solution to mitigate lateral spreading of soils during liquefaction [Arulmoli *et al.*, 2004; Boulanger *et al.*, 2006; Elgamal *et al.*, 2009; Rayamajhi *et al.*, 2014]. Installing reinforcement piles in liquefiable ground can reduce permanent lateral deformation in soils due to pile-pinning effects. It appears to be equally effective for the sand and the silt strata [Elgamal *et al.*, 2009]. On the other hand, stone column procedure has significantly low efficiency for silty grounds due to low permeability of silts.

Numerical simulation is an important tool to assess the effectiveness and efficiency of ground improvement methods. For example, sensitivity analyses [Maheshwari and Sarkar, 2011] have been carried out to study seismic response of a single pile or pile groups in liquefiable soils using finite element program. The numerical studies demonstrated that

CONTACT Gang Wang gwang@ust.hk Department of Civil and Environmental Engineering, Hong Kong University of Science and Technology, Clear Water Bay, Hong Kong, China.

Color versions of one or more of the figures in the article can be found online at www.tandfonline.com/ueqe.

seismic response of the soil–pile system is largely influenced by spacing of pile groups, ratios of pile–soil rigidity, peak amplitude, and frequencies of input acceleration time histories. Elgamal *et al.* [2009] and Asgari *et al.* [2013] also used 3D finite element simulations to investigate key design parameters for the pile-reinforcement approach, including the influence of pile-replacement ratios and ground-motion characteristics on the soil deformation. In these studies, the diameter of piles was assumed as 0.6 m, but the effects of using different pile diameters have not yet been investigated. The base of piles is assumed to be fixed, i.e., no displacement and rotation are allowed around the pile tip. The assumption leads to maximum bending moment concentrated at the pile tip. On the other hand, a number of studies [Phanikanth *et al.*, 2013] assumed a floating tip condition in their analysis of a single pile pinning through a liquefied layer, which means the bending moment at the tip of the pile is always zero. Apart from numerical studies, centrifuge tests have been conducted to investigate the efficacy of ground improvement with an emphasis on modeling the fluid-like behavior of liquefied soils around piles [Takahashi *et al.*, 2016].

The embedment condition of the reinforcement piles is still a subject of controversy in various numerical schemes, which may greatly influence the effectiveness of the pile reinforcement in the liquefied ground. The fixed-end condition for reinforcement piles, as adopted in most literature, is only appropriate for an idealized case that the piles are socketed into a solid rock. In reality, soils underlying the liquefiable layer may be less competent than a solid rock. However, the influence of pile-embedment condition has not yet been well studied.

In this paper, fully nonlinear finite element analyses are conducted to study the effectiveness of pile reinforcement in liquefiable multi-layered soils under earthquake loading. Parametric studies are conducted by varying pile-embedment length into denser strata in multi-layered soils, as well as different area replacement ratios and pile diameters. Based on numerical studies, practical recommendations are proposed for pile layout and pile-embedment length in different soil profiles, which is useful to improve the effectiveness of pile reinforcement in the liquefied ground.

2. Computational Model

2.1. *Model Geometry and Soil Properties*

In this study, OpenSeesPL [Lu *et al.*, 2011a], a finite element program is used to study the pile-reinforcement effects for liquefied ground. This computational framework has been actively used in many pile–soil interaction analyses in recent years [Elgamal *et al.*, 2009; Wang and Sitar, 2011; Asgari *et al.*, 2013]. Figure 1 shows the schematic plan view of ground layout with circular piles installed in a periodic pattern. If the ground shaking direction is specified as shown in Fig. 1a, a periodic unit cell can be used to represent the soil–pile interaction due to symmetry of the setup. The unit cell has two periodic displacement boundaries on both sides, and two symmetric boundaries along the shaking direction. Due to symmetry, the nodes along the symmetry boundaries can only displace in the shaking direction as illustrated in Fig. 1b. The corresponding nodes on the two periodic boundaries are tied together so that they will have identical movement. The periodic unit cell greatly simplifies the numerical simulation, as it represents a large remediated ground area. In this case, the area replacement ratio A_{rr} is defined as the area of the pile to the tributary area following Eq. (1):

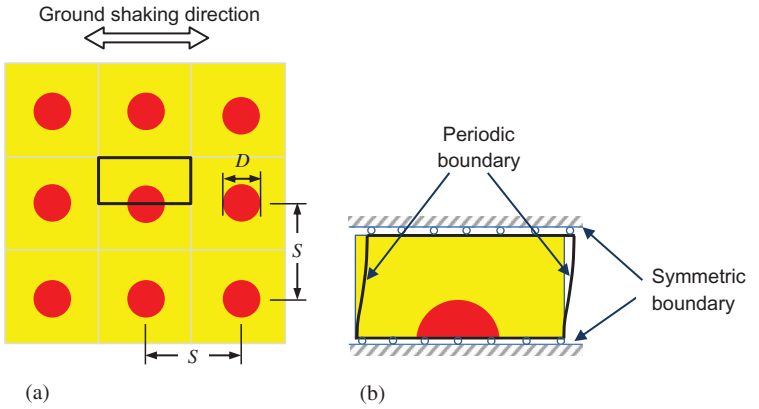

Figure 1. (a) Plan view of pile layout; and (b) a periodic unit cell.

$$A_{rr} = \frac{\pi D^2}{4S^2} \tag{1}$$

where D denotes the pile diameter and S is the spacing between centers of piles.

The pressure-dependent multi-yield-surface plasticity constitutive model [Yang *et al.*, 2003] is used to model the behaviors of liquefiable soil in the current study. The model has been used in a number of numerical studies on pile–soil interaction in liquefiable ground [e.g., Lu *et al.*, 2011b]. There are several features associated with the constitutive model: (a) The yield surfaces of the soil are pressure-dependent, as shown in Fig. 2a as nested cones in the principal stress space. The outermost surface is the envelope of peak shear strength (failure envelope). The nested yield surfaces form the hardening zone in the context of multi-surface plasticity to simulate nonlinear soil behaviors. (b) The model can properly model shear-induced dilatancy during liquefaction process. The model specifies the soil to be contractive if the stress is within a phase-transformation (PT) surface, and dilative if the stress is beyond the PT surface, as shown in Fig. 2b.

Table 1 summarizes the main constitutive model parameters for loose, medium, and dense sands that are used throughout this study. Major model parameters include mass

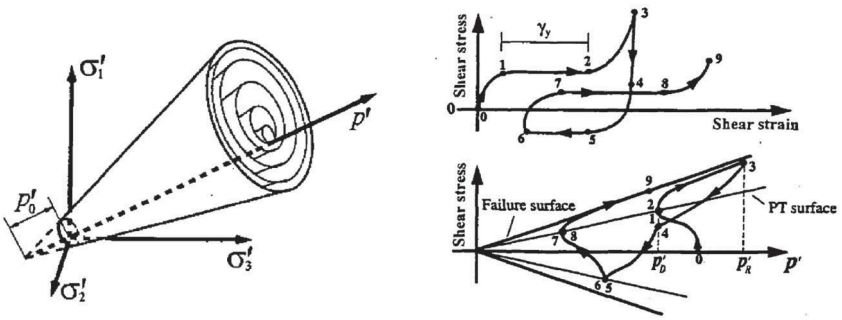

(a) Conial yield surface in principal stress space (b) Stress-strain and stress path

Figure 2. Pressure-dependent multi-yield-surface plasticity constitutive model [after Yang *et al.*, 2003; Elgamal *et al.*, 2003].

density (ρ), low-strain shear modulus (G_r), and friction angle (ϕ) to quantify typical dynamic soil properties. The variation of shear modulus is defined as a function of effective confining pressure using the reference low-strain shear modulus. More importantly, soil dilatancy is specified using contraction and dilation constants (c_1, d_1, and d_2), which also control the pore-pressure buildup rate of soils in the liquefaction process. In general, the loose sand appears to be more contractive than the dense sand. Therefore, they are more prone to liquefaction. Note that the model parameters in Table 1 represent typical loose, medium, and dense sands, which have also been extensively calibrated using monotonic and cyclic laboratory tests [Lu *et al.*, 2011a].

Figure 3 shows an example of the finite element modeling of the unit cell with a pile embedded in two-layer soil strata. As shown in Fig. 3a, the top layer is 10 m underlain by a 6 m bottom layer. The reinforcement piles are embedded into the bottom soil by a specified embedment length. The soil domain is discretized using eight-node brick elements with *u-p* formulation [cf. Zienkiewicz *et al.*, 1990; Xie and Wang, 2014] such that water pressure and soil deformation can be solved simultaneously. Beam elements are used to model the pile in order to accurately capture its bending behaviors. Since the beam element has no radial dimension, the actual diameter of the pile is modeled using rigid links placed normal to the pile axis, as shown in Fig. 3b. Furthermore, the rigid links form node-to-node contact with the surrounding soil elements, so contact and spacing between the pile and soils can be

Table 1. Model parameters of loose, medium and dense sands used in this study.

Parameter	Loose sand	Medium sand	Dense sand
Mass density (ρ)	1700 kg/m^3	1900 kg/m^3	2100 kg/m^3
Reference low-strain shear modulus (G_r)	55 MPa	75 MPa	130 MPa
Friction angle (ϕ)	29°	33°	40°
PT angle (ϕ_{PT})	29°	27°	27°
Contraction parameter (c_1)	0.21	0.07	0.03
Dilation parameters (d_1 and d_2)	0.0 and 0.0	0.4 and 2.0	0.8 and 5.0

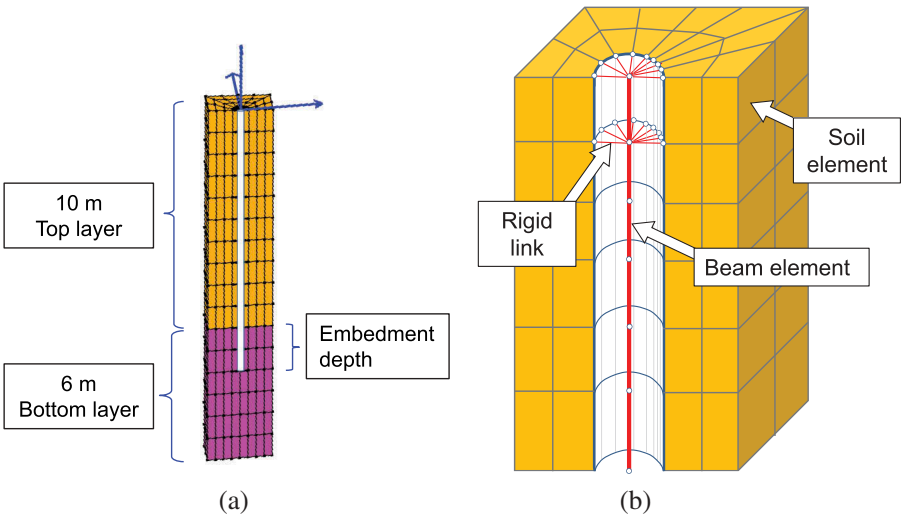

Figure 3. (a) Finite element modeling layout of the unit cell; and (b) details of pile–soil interaction model and mesh configuration.

realistically simulated. The water table is assumed to be at the ground level; therefore, the soil profile is fully saturated. The ground is assumed to be mildly sloping with an inclination angle of 4°.

Given that pile damage is not within the scope of the present study, the concrete pile is assumed to be linearly elastic with a typical mass density of 2.4×10^4 kg/m^3 and Young's modulus E of 20 GPa. The pile head is free as no pile cap or deck is included in this case. In addition, as the pile is used for ground improvement, it does not take axial load.

2.2. *Input Ground Motions*

In this study, two acceleration time histories are used as input motions for the numerical analyses. The two motions are recorded during the 1940 Imperial Valley earthquake at the El Centro station (termed as "El Centro motion" throughout this study) and the 1989 Loma Prieta earthquake at the Treasure Island station (termed as "Loma Prieta motion"), respectively. Figure 4 compares the acceleration time histories, Arias intensity buildup and Fourier spectra of the two input motions, which were linearly scaled to peak ground acceleration of 0.35 g. As shown in Table 2, durations of two input motions differ significantly. The number of significant excitation cycles is 14.5 for the El Centro motion, as is compared with 5.8 cycles for the Loma Prieta motion. In addition, the energy flux for scaled Loma Prieta motion is 5784 J m^{-2} s^{-1}, which is about twice as much as that of the scaled El Centro motion (2469 J m^{-2} s^{-1}).

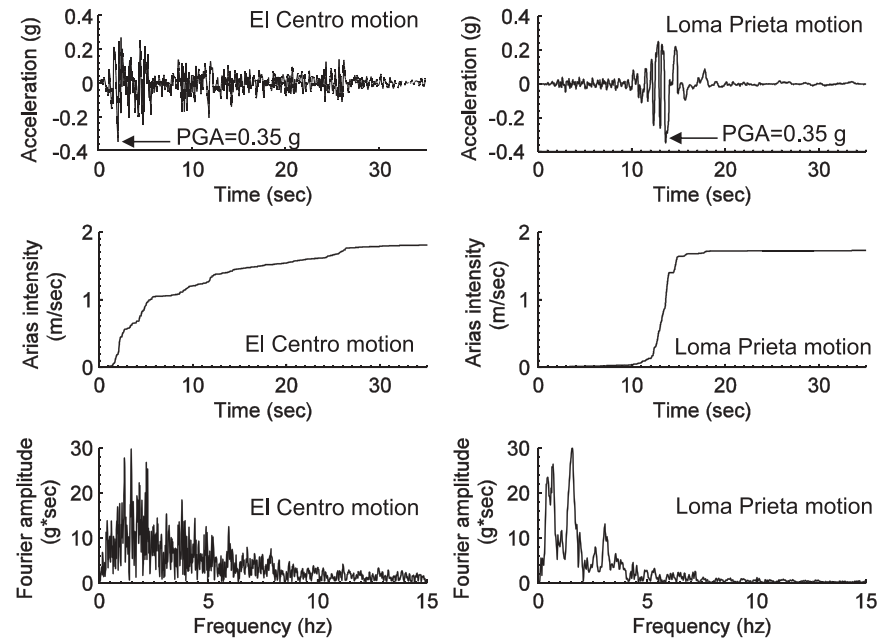

Figure 4. Acceleration time histories, Arias intensity buildup and Fourier spectra of the input motions: (a) the El Centro motion and (b) the Loma Prieta motion. Both records are scaled to peak ground acceleration (PGA) = 0.35 g.

Table 2. Parameters of the two ground-motion records used in this study.

Parameters	El Centro motion	Loma Prieta motion
Date of the event	18/05/1940	18/10/1989
Recording station	El Centro	Treasure Island
Moment magnitude of the event	7.1	6.9
Significant duration, D_{5-95} (s)	24.4	4.4
Significant duration, D_{5-75} (s)	10.5	2.7
Energy flux for scaled records (J m^{-2} s^{-1})	2469	5784
Number of significant excitation cycles, N_c	14.5	5.8

Notes: D_{5-75} and D_{5-95} denote the time interval over which 5–75% and 5–95% of the Arias intensity is accumulated, respectively [Du and Wang, 2017]; N_c is the equivalent number of uniform cycles at 65% of the peak acceleration [Idriss and Boulanger, 2008].

3. Reinforcement Using Fixed-End Piles

3.1. *Reinforcement Effect of Fixed-End Piles*

In this section, numerical simulations were performed to demonstrate the mitigation effect of fixed-end pile groups on lateral displacement of liquefied ground. In the simulation, it is assumed that the pile, with a diameter D = 0.6 m, is fixed at the base of the computation domain, representing the case that the pile is firmly socked into a rigid rock. The liquefiable soil is assumed to be 10 m in depth. First, simulations are conducted for piles in a loose sand, with the area replacement ratio of piles A_{rr} changing from 0% (free field) to 20%. Figure 5 shows the lateral displacement of the surface soil (close to the pile) under the El Centro motion. The permanent ground displacement when A_{rr} = 0 reaches above 1 m, providing a reference of free-field response in comparison with the pile reinforcement cases. It is worth mentioning that the pile group with 1% A_{rr} can be already beneficial to reduce lateral ground deformation to 0.2 m, as can be seen in Fig. 5. As A_{rr} gradually increases to 5%, permanent ground displacement significantly reduces to around 0.1 m, which was found to possibly provide satisfactory mitigation effect.

Ground reinforcement with the fixed-end piles (shown in Fig. 6a) is clearly effective in reducing the ground displacement for the reason that the soil movement is pinned by the pile. Using pile diameter D = 0.6 m and an area replacement ratio A_{rr} = 5%, Fig. 6b shows the maximum lateral displacement of the fixed-end pile installed in loose, medium, and dense sands, respectively, under the El Centro motion. It is obvious that there is no pile rotation at the fixed end. Bending moment and shear force in the pile reach the maximum values at the fixed end, as shown in Fig. 6c,d, while they are practically zero at the ground surface.

Figure 7 shows excess pore water pressure time histories in the loose, medium, and dense sand at 4.79 m depth, 0.3 m from the pile center under the El Centro motion. The generation of excess pore pressure is closely related to the initiation of liquefaction. Liquefaction occurs in the soil when buildup of excessive pore pressure equals to the total mean stress. For loose, medium, and dense sands, liquefaction was initiated at around 2 s, 5 s, and 12 s, respectively (highlighted with triangles in Fig. 7). Figure 8 further illustrates shear stress–strain curves and stress paths in loose, medium, and dense sands. Under cyclic loading, the stress path moves to the left until it reaches "zero" effective stress, leading a large soil deformation up to 2% in loose and medium sands. During the post-liquefaction process, flow deformation is also accompanied by strain

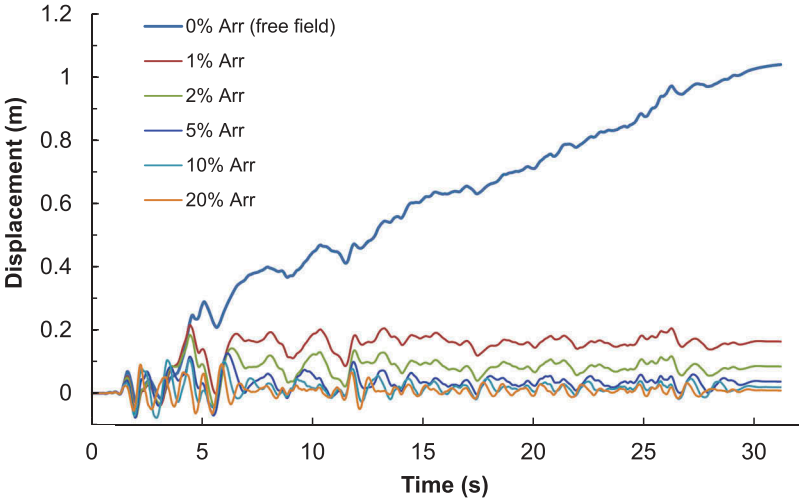

Figure 5. Ground surface lateral displacement time histories for loose sand, A_{rr} from 0% (free field) to 20% under the El Centro motion.

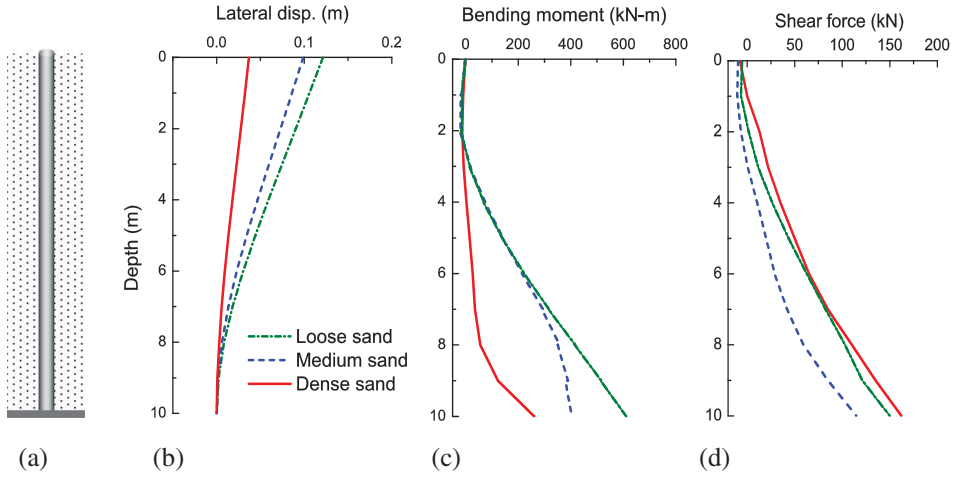

Figure 6. (a) A fixed-end pile in a 10 m deep soil in the unit cell (D = 0.6 m, A_{rr} = 5%); (b) maximum lateral displacement, (c) envelop of maximum bending moment, and (d) maximum shear force distribution, for the fixed-end pile in loose, medium and dense sands under the El Centro motion.

hardening when the soil dilates and stress increases along the failure envelop. Clearly, installing the fixed-end piles in the soil stratum cannot prevent soils from liquefaction, but is definitely effective to reduce the ground lateral displacement.

Similar tests have been conducted for loose, medium, and dense sands reinforced by fixed-end piles under the Loma Prieta motion (pile diameter 0.6 m and the area replacement ratio 5%). Figure 9 shows the maximum lateral displacement, bending moment, and shear force distribution along the piles, which have similar patterns but the amplitudes are more than twice as much as the El Centro case. The difference may be attributed to the

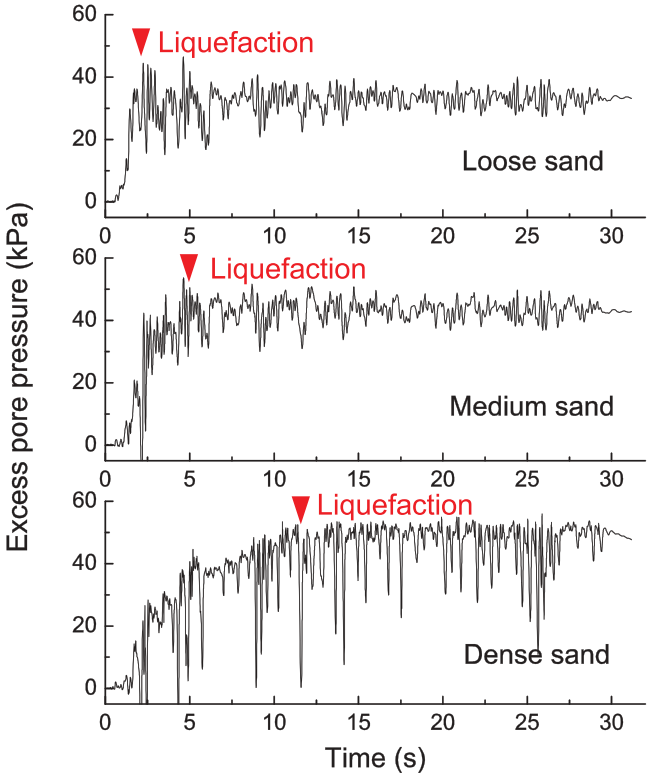

Figure 7. Excess pore water pressure time histories in loose, medium and dense sand at 4.79 m depth, 0.3 m from the center of the fixed-end pile (D = 0.6 m, A_{rr} = 5%) under the El Centro motion.

energy flux of two input motions. The stress–strain curves and stress paths in soils (Fig. 10) are also similar to the El Centro case (Fig. 8).

3.2. *Influence of Pile Diameter on Ground Lateral Displacement*

In this section, the effect of pile diameter D on ground lateral displacement under seismic loading is investigated. The configuration of a single-layer soil and the fixed-end pile is shown in Fig. 6a. By fixing the area replacement ratio A_{rr} to 10%, the pile diameter is set as 0.2 m, 0.3 m, 0.4 m, 0.5 m, 0.6 m, 0.8 m, 1 m, 2 m, and 3 m, respectively. The horizontal dimension of the computational domain (i.e., the pile spacing) has to be adjusted accordingly in order to keep the same area replacement ratio (A_{rr} = 10%) for cases of different pile diameters.

Figure 11 shows the maximum pile displacement and soil displacement at ground level for piles with different diameters under the El Centro motion. It can be observed that in general piles with a large diameter would have smaller maximum displacement while keeping A_{rr} constant. When the pile diameter is 0.2 m, the maximum pile displacement is 0.19 m. The value is reduced to below 0.05 m when the pile diameter is greater than 0.6 m. The trend can be well explained by examining the total stiffness of piles: as the flexural rigidity of a fixed-end pile $EI = E\pi D^4/64$, the number of piles in a specified area is 4 ×

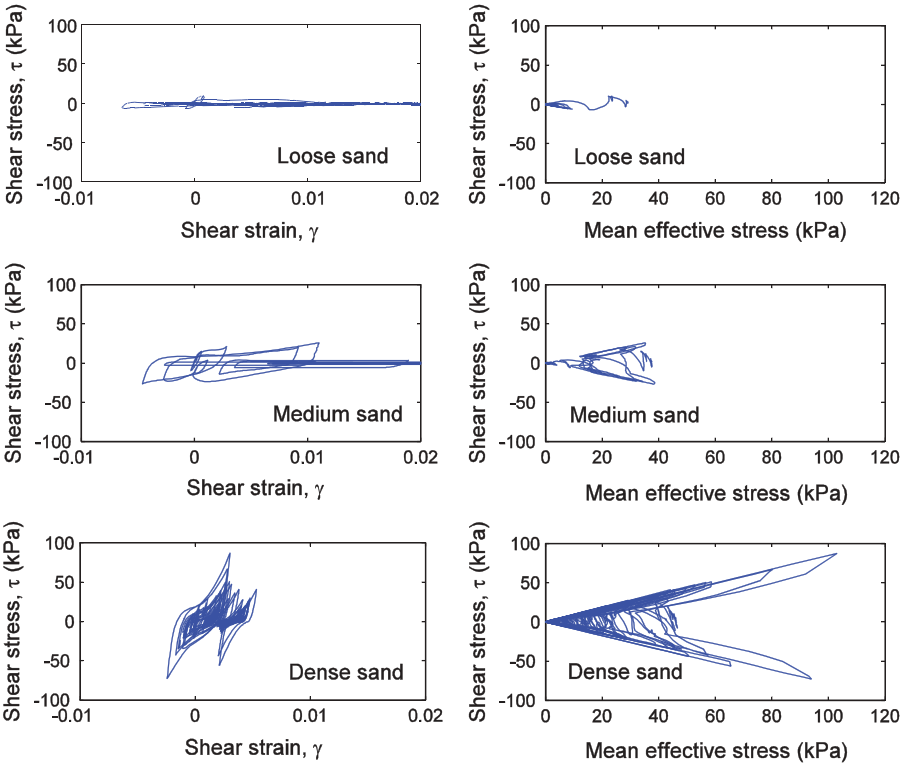

Figure 8. Shear stress–strain curves and stress path for loose, medium and dense sands at 4.79 m in depth, 0.3 m from the pile center under the El Centro motion.

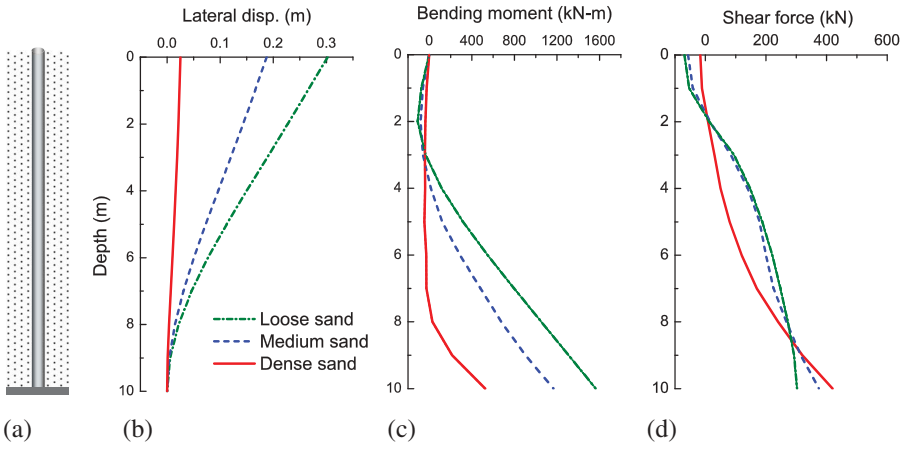

Figure 9. (a) A fixed-end pile in a 10 m deep soil in the unit cell (D = 0.6 m, A_{rr} = 5%); (b) Maximum lateral displacement, (c) envelop of maximum bending moment, and (d) maximum shear force distribution, for the fixed-end pile in loose, medium and dense sands under the Loma Prieta motion.

Area/πD^2. Therefore, the total flexural rigidity of piles per unit area ($EI \times N$/Area) is proportional to D^2, resulting in decrease in the maximum pile displacement when the pile diameter increases, as shown in Fig. 11a.

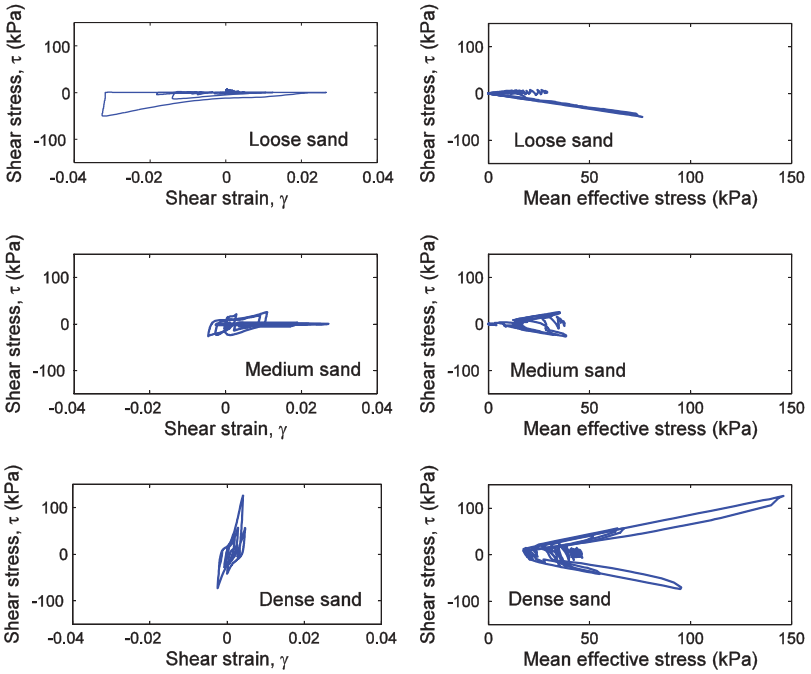

Figure 10. Shear stress–strain curves and stress path for loose, medium and dense sands at 4.79 m in depth, 0.3 m from the pile center under the Loma Prieta motion.

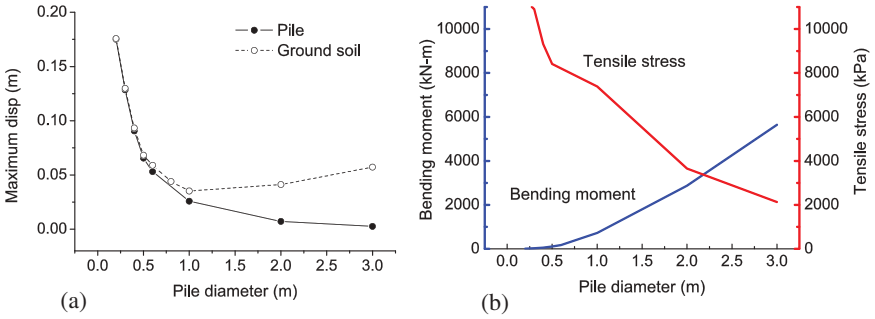

Figure 11. (a) Maximum pile displacement and ground displacement; and (b) maximum bending moment and maximum tensile stress versus pile diameter.

On the other hand, the relation between maximum ground displacement and pile diameter is also illustrated in Fig. 11a. For the cases of small-diameter piles, the piles are closely spaced, which means that the soil is constrained and moves together with piles. Therefore, the maximum ground soil displacement decreases first with increasing pile diameter. Interestingly, the maximum ground displacement begins to increase when pile diameter is larger than 1 m. This is because when pile spacing becomes large, they may not be able to effectively constrain the movement of soils.

Figure 11b shows that the maximum bending moment in the pile increases significantly with increasing pile diameter, approaching to 6000 kN m for a 3-m diameter pile. The

maximum tensile (or compressive) stress can be estimated using $\sigma_t = M \cdot r/I$, and $I = \pi r^4/4$, where M is the bending moment and r is the pile radius. Figure 11b shows the larger diameter, the smaller tensile stress is induced in the pile. The stress analysis provides useful information to determine the amount of rebar in the reinforced concrete piles. Results from the Loma Prieta motion show a similar trend as that of the El Centro motion case, which will not be reported here.

4. Effects of Pile-Embedment Length in Layered Soil Strata

4.1. *Soil Strata and Model Setup*

For most cases, the assumption of a fixed end for the pile cannot be satisfied, since deep soil strata may underlie the liquefiable soil instead of a solid rock. In this study, numerical models are developed with piles embedded into a denser soil stratum. The influence of pile-embedment length on ground lateral displacement, and shear and bending moment of piles is investigated through parametric analyses. The pile employed in the simulation is circular with a fixed diameter of 0.6 m, and the area replacement ratio A_{rr} is assumed to be 5%. The horizontal dimension of the unit cell is 2.38 m. Mesh in the vertical direction is uniformly divided as 1 m in size, so the numerical simulation can effectively capture the wave frequency greater than 10 Hz.

Figure 12 shows configuration of the two-layer soil strata and piles embedded into a denser stratum with embedment length varied from 0 m, 1 m, 2 m, 3 m, 4 m, and 5 m. The upper layer is either loose or medium sand of 10 m in depth. The lower 6 m layer can be liquefiable or non-liquefiable but has a higher density than the upper layer. The properties of the sands adopted in this analysis are shown in Table 1. Three simulation cases are summarized in Table 3, which are termed as Cases LM, LD, and MD, respectively. Note that "L", "M", and "D" stand for "loose", "medium", and "dense" sands. The first letter denotes the upper layer and the second letter is for the lower layer.

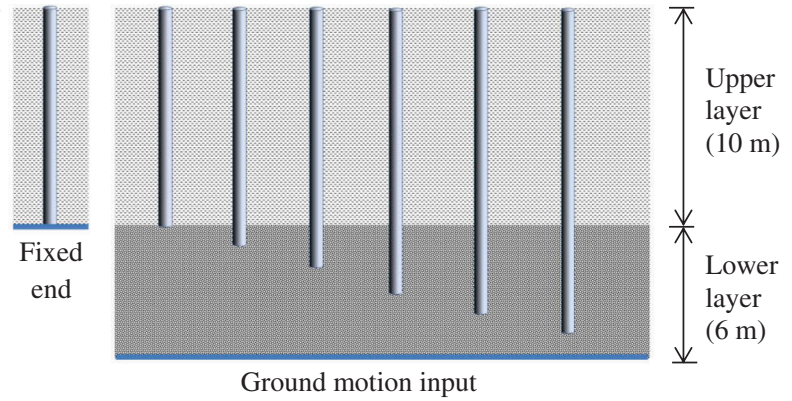

Figure 12. Soil strata, fixed-end pile and floating piles embedded into a denser stratum with varied embedment length.

Table 3. Three types of soil profiles used in this study.

Simulation Cases	Upper Soil Layer	Lower Soil Layer
Case LM	Loose sand	Medium sand
Case LD	Loose sand	Dense sand
Case MD	Medium sand	Dense sand

4.2. *Development of Excess Pore Water Pressure and Stress–Strain in Soils*

4.2.1. *Response under the El Centro Motion*

Excess pore water pressure is a key indicator for the development of soil liquefaction. Figure 13 illustrates the excess pore-pressure generation along the soil depth for the LD case under the El Centro motion. Two cases are compared: the first is a free-field condition without pile installation, and the second case is for piles embedded 3 m into the underlying dense sand. The initial effective vertical stress line $\sigma'_v = \gamma' h$ is also plotted for reference, where γ' is the submerged unit weight of the loose sand and h is the soil depth. For both cases, the development of excessive pore pressure is similar in the upper 10 m of loose sand layer. Within 3 s, the excess pore water pressure approaches the initial effective stress line, indicating complete liquefaction of the upper layer. Again, the results demonstrated installation of piles would not significantly influence development of excess pore water pressure; thus, the initiation of liquefaction in the loose sand. As will be further discussed, liquefaction triggering occurs at a strain level less than 1%, while shaking-induced strains in the soil well exceed this level even if piles are installed.

Figure 14 compares the stress–strain curves of soils at different depths. Small strain and large shear resistance is mobilized in the soil (1.19 m from the pile center) before liquefaction. After the initial liquefaction, quite large flow deformation occurs in the soil if no pile is installed, where the strain can reach as much as 130% at the depth of 8.79 m, as shown in Fig. 14a. In the post-liquefaction, strain hardening is also observed as the soil dilates during flow deformation, and the soil completely loses its shear resistance upon unloading. The phenomenon has been attributed to the development of highly anisotropic

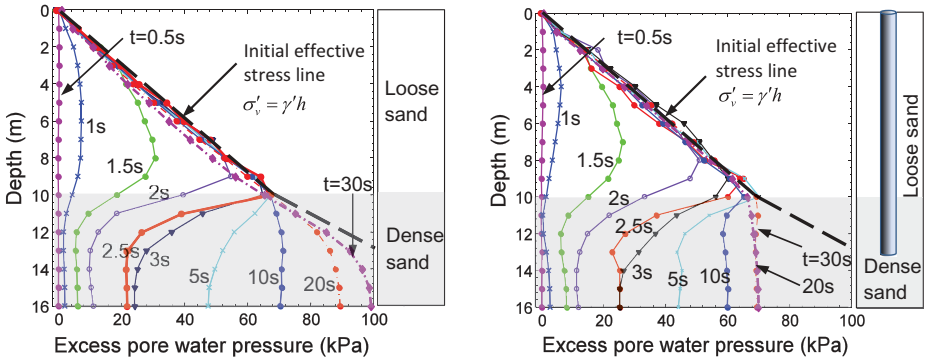

Figure 13. Distribution of excess pore water pressure along soil depth (1.19 m from the pile center) under the El Centro motion for the LD case: (a) no pile installed and (b) piles installed with embedment length of 3 m into the dense sand.

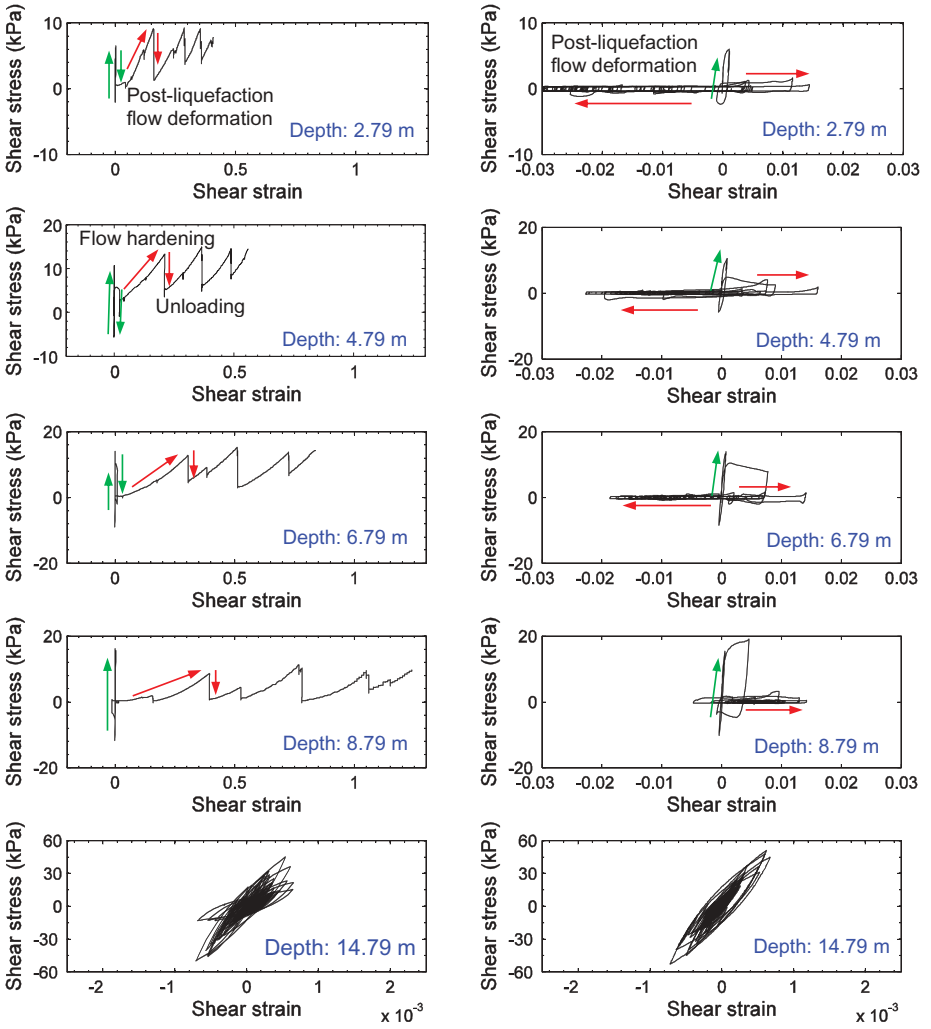

(a) No pile installed (b) Piles installed with embedment length 3m

Figure 14. Shear stress–strain curves along soil depth (1.19 m from the pile center) under the El Centro motion for the LD case: (a) no pile installed and (b) piles installed with embedment length 3 m into the dense sand.

microstructure in the post-liquefaction process [Wang and Wei, 2016; Wei *et al.*, 2018]. With piles installed and embedded 3 m into the dense layer, the reinforcement piles provide significant constraint to the post-liquefaction deformation of the soil. The maximum post-liquefaction strain is only around 2–3% in various depths. It should be noted that small residual strength of around 0.5 kPa is developed in the soil when flow deformation occurs, as shown in Fig. 14b.

Figure 15 shows the shear strain distribution along soil depth (1.19 m from the pile center) for the LD case under the El Centro motion. For the case with no piles installed (Fig. 15a), large shear strain mainly occurs in the loose sand. After initiation of liquefaction (3 s), the shear strains begin to concentrate along the interface of the loose and the

dense strata. The strains accumulate progressively and reach 130% till 30 s along the sloping direction. When piles are installed but are not embedded into the dense sand (Fig. 15b), large rotation of the pile could occur around the tip. One can further refer to Figs. 18–19 for pile displacement profile. Accordingly, soil strain distribution in the loose sand becomes more uniformly distributed along the depth, which is constrained by the rotation and displacement of the pile. The maximum strain in the soil is as large as 15% as shown in Fig. 15b. On the other hand, the maximum shear strain in the soil can be significantly reduced if the piles are embedded into a dense stratum, because the embedment constrains movement and rotation of the pile. In Fig. 15c, the maximum shear strain in the soil is less than 6% when the pile is embedded 3 m into the dense sand.

From the above observation, it is evident that the embedment length is a critical design parameter for pile reinforcement. As is summarized in Fig. 15d, if the embedment length is zero, a large lateral soil displacement at the ground level is observed (around 1 m), showing that the mitigating effect is minimal even when piles are installed. As pile-embedment length reaches more than 2 m, permanent ground displacement can be effectively reduced to below 0.2 m.

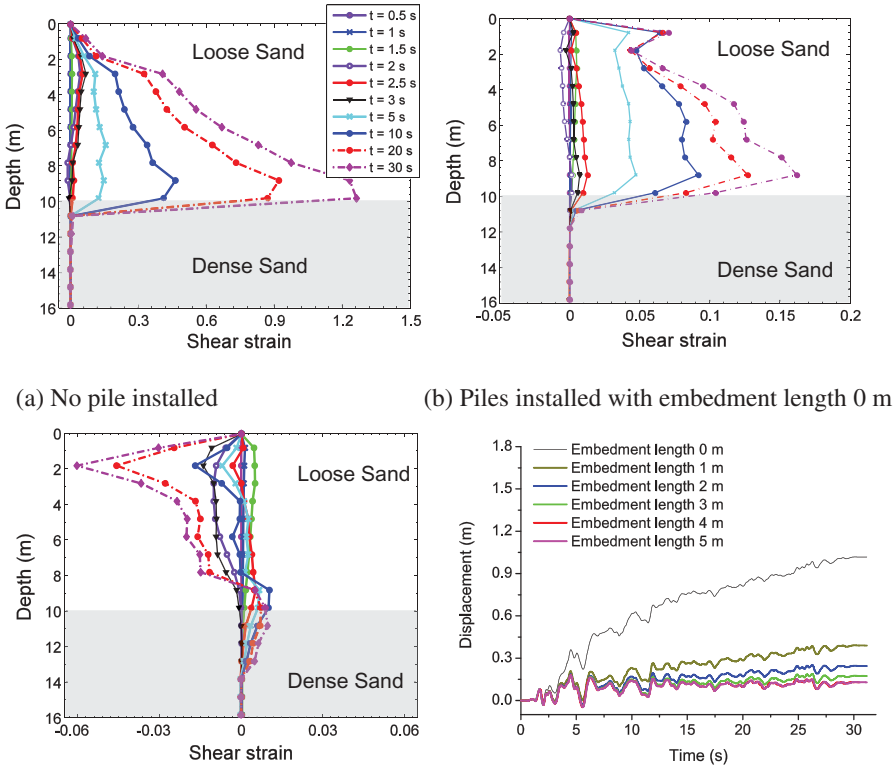

(a) No pile installed (b) Piles installed with embedment length 0 m

(c) Piles installed with embedment length 3 m (d) Displacement time histories of soils

Figure 15. Distribution of shear strain along soil depth (1.19 m from the pile center) under the El Centro motion for the LD case: (a) no piles installed, (b) piles installed with an embedment length of 0 m, (c) piles installed with an embedment length of 3 m into the dense sand, and (d) lateral displacements time history in the soil at ground level for different embedment length.

4.2.2. *Response under the Loma Prieta motion*

Figure 16 shows stress–strain curves along soil depth for the LD case under the Loma Prieta motion. Similar to results of the El Centro case (Fig. 14), large flow deformation occurs in the soil after the initial liquefaction when no pile is installed (Fig. 16a), where the strain reaches 80% at the depth of 8.79 m, while for the case with piles installed with embedment length of 3 m (Fig. 16b), the maximum strain is around 4%. In general, the pattern of post-liquefaction flow deformation is comparable to the El Centro case. The reinforcement effect of piles is demonstrated to be significant.

Figure 17 shows the shear strain distribution along soil depth under the Loma Prieta motion. The case once again demonstrates that the embedment length is significant for the pile mitigation effect similar to the El Centro case. If no pile is installed, the shear strain in the soil profile accumulates increasingly to 80% at 30 s (Fig. 17a). When piles are installed but are not embedded into the dense layer, the shear strain is developed progressively to 9%, shown in Fig. 17b. On the other hand, the maximum shear strain is around 4% when the pile is embedded 3 m into the dense layer, shown in Fig. 17c. Note that most of shear

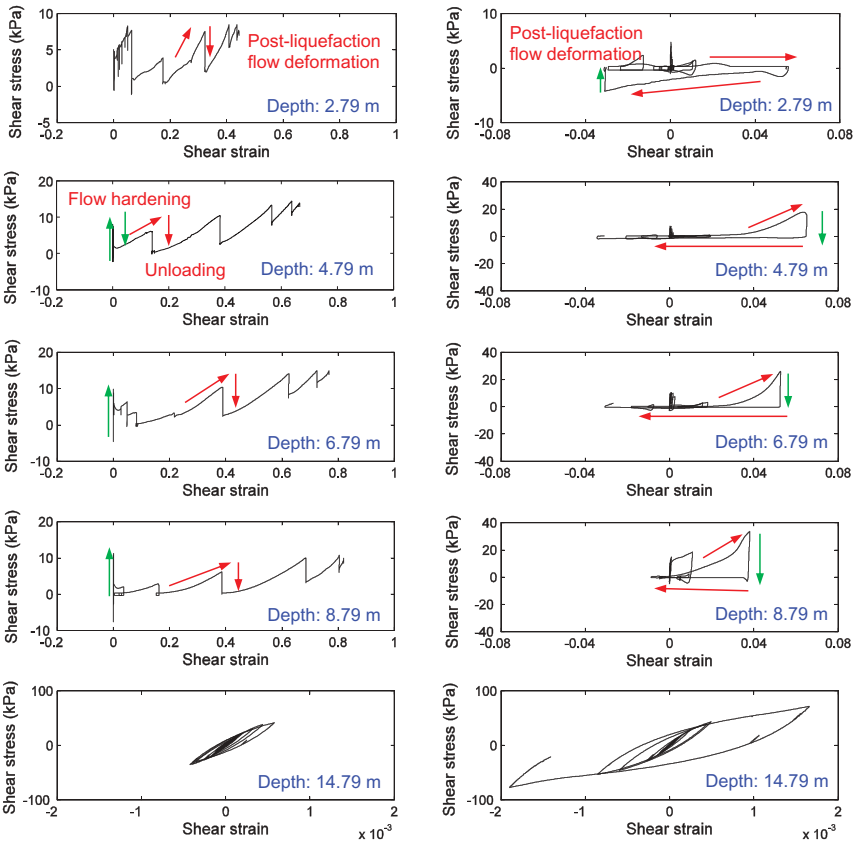

(a) No pile installed (b) Piles installed with embedment length 3m

Figure 16. Shear stress–strain curves along soil depth (1.19 m from the pile center) under the Loma Prieta motion for the LD case: (a) no pile installed and (b) piles installed with embedment length 3 m into the dense sand.

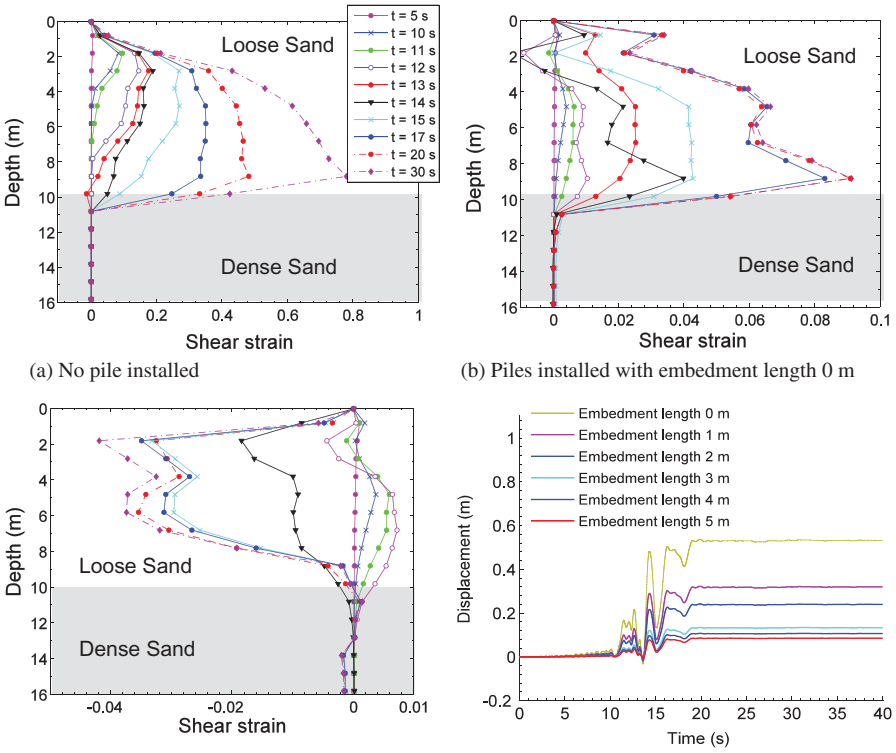

(a) No pile installed

(b) Piles installed with embedment length 0 m

(c) Piles installed with embedment length 3 m

(d) Displacement time histories of soils

Figure 17. Distribution of shear strain along soil depth (1.19 m from the pile center) under the Loma Prieta motion for the LD case: (a) no piles installed, (b) piles installed with an embedment length of 0 m, (c) piles installed with an embedment length of 3 m into the dense sand, and (d) lateral displacements time history in the soil at ground level for different embedment length.

strains are developed during 10–17 s of the Loma Prieta motion, which corresponds to most of its Arias intensity accumulation (Fig. 4b).

4.3. *Effects of Embedment Length*

Figures 18 and 19 show the maximum lateral displacement profiles of the piles for simulation cases of the fixed end, and Cases LM, LD, MD under the Loma Prieta and El Centro ground motions. The fixed-end pile results in a minimum lateral displacement as the pile tip is fixed and no rotation is allowed during the seismic loading. On the other hand, the pile with zero embedment length reaches a largest lateral displacement, as the pile tip is subjected to movement and rotation without being embedded into a denser layer. The simulations demonstrated that the fixed-end assumption can be unconservative in estimating the pile-reinforcement effects, while piles with zero embedment length are virtually not effective. In general, increasing pile-embedment length into a stiffer underlying layer can reduce the lateral displacement. The overall lateral pile displacement is the highest for Case LM, followed by Case LD, and the smallest for Case MD.

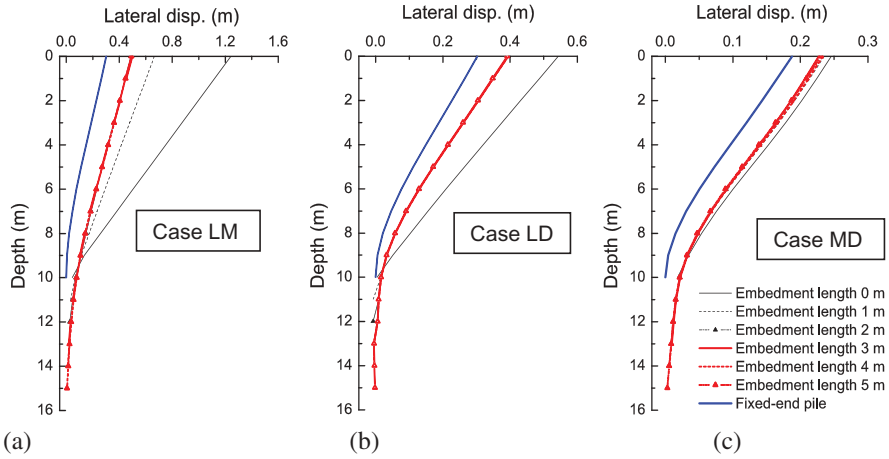

Figure 18. Maximum lateral displacement profile of the piles under the Loma Prieta motion for the three computation cases: (a) LM, (b) LD, and (c) MD.

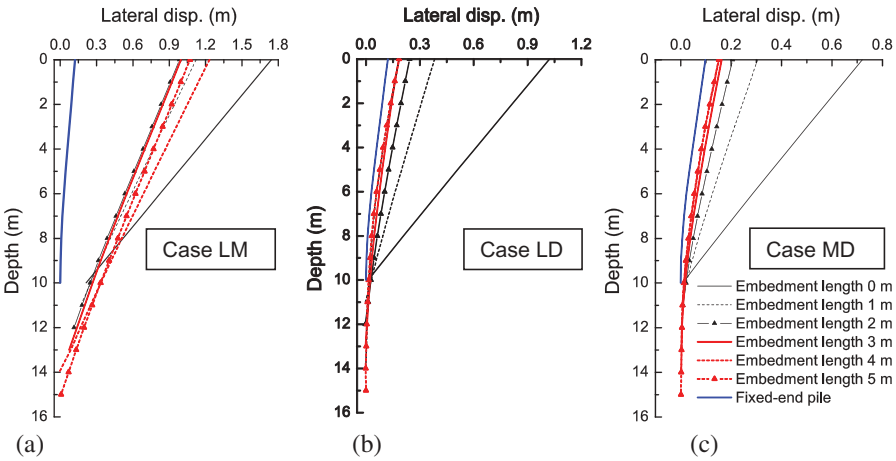

Figure 19. Maximum lateral displacement profile of the piles under the El Centro motion for cases: (a) LM, (b) LD, and (c) MD.

The effects of embedment length on the maximum lateral displacements at the ground level are summarized in Fig. 20 and Table 4. In general, increasing the embedment length will reduce the maximum lateral ground displacement, while the improvement will become less significant if the embedment length is over 2 m. If the underlying layer is dense sand (Cases LD, MD), the maximum displacement monotonically reduces and approaches the fixed-end pile cases. For both cases, it is recommended that the piles should be embedded at least 1 m into the dense sand.

The Case LM corresponds to the largest ground displacements because the underlying medium sand is less competent than the dense sand. For the Case LM under the El Centro motion, the ground displacement is greater than 1 m even if the embedment length is up

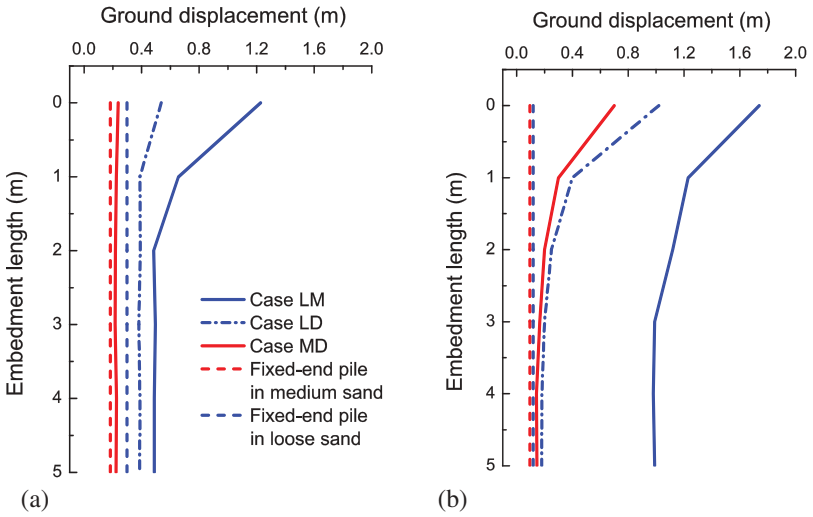

Figure 20. Maximum lateral displacements at the ground surface versus pile-embedment length under: (a) the Loma Prieta motion and (b) the El Centro motion.

Table 4. Maximum ground surface lateral soil displacement for different embedment length.

Simulation Case	Input motion	Soil displacement (m) Embedment length 0 m	Embedment length 1 m	Embedment length 2 m	Recommended embedment length
Case LM	Loma Prieta	1.23	0.66 (46%)	0.48 (61%)	2 m
	El Centro	1.73	1.23 (29%)	1.12 (35%)	
Case LD	Loma Prieta	0.54	0.39 (28%)	0.39 (28%)	1 m
	El Centro	1.02	0.39 (62%)	0.27 (74%)	
Case MD	Loma Prieta	0.24	0.22 (9%)	0.22 (9%)	1 m
	El Centro	0.70	0.29 (59%)	0.22 (69%)	

Note: Values in parentheses show percentage of reduction compared with the zero embedment case.

to 5 m. It is recommended the embedment length should be at least 2 m into the medium sand.

Figure 21 illustrates the maximum bending moment profile in piles for the Case LD. The maximum bending moment along the pile always occurs at the interface between the upper and lower soil layers (10 m in depth), and increases with embedment length. Figure 22 presents the maximum bending moment along the pile versus embedment length. In all cases, Case LD has the highest overall maximum moment along the pile. The bending moment calculated using fixed-end piles in medium and loose sands are also plotted in Fig. 22, providing a reference for embedded piles. It can be observed that the maximum moment increases as embedment length increases but will be smaller than the fixed-end case.

Figure 23 presents the maximum shear force along the pile versus embedment length. It can be observed that Case LD has the highest overall maximum shear force along the pile

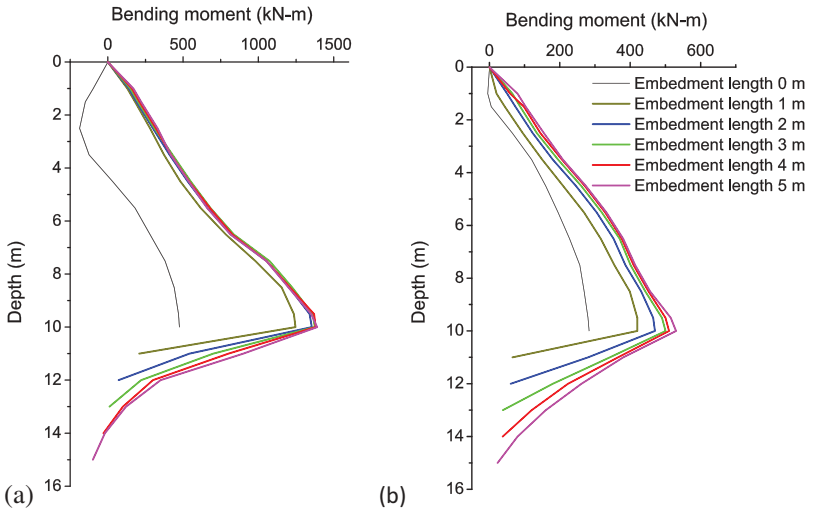

Figure 21. Maximum bending moment profile in piles for Case LD under: (a) the Loma Prieta motion and (b) the El Centro motion.

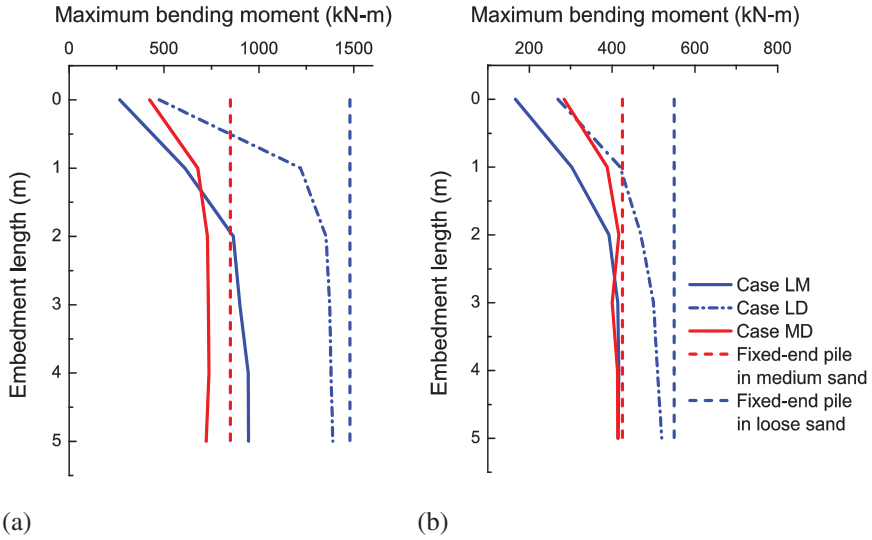

Figure 22. Maximum bending moment along pile versus pile-embedment length under: (a) the Loma Prieta motion and (b) the El Centro motion.

for both earthquakes. The maximum shear force first increases and reaches a maximum value at 1 m embedment and then decreases to progressively as the embedment length further increase. Also, Loma Prieta motion creates higher shear force than the El Centro motion, this is true for all cases investigated.

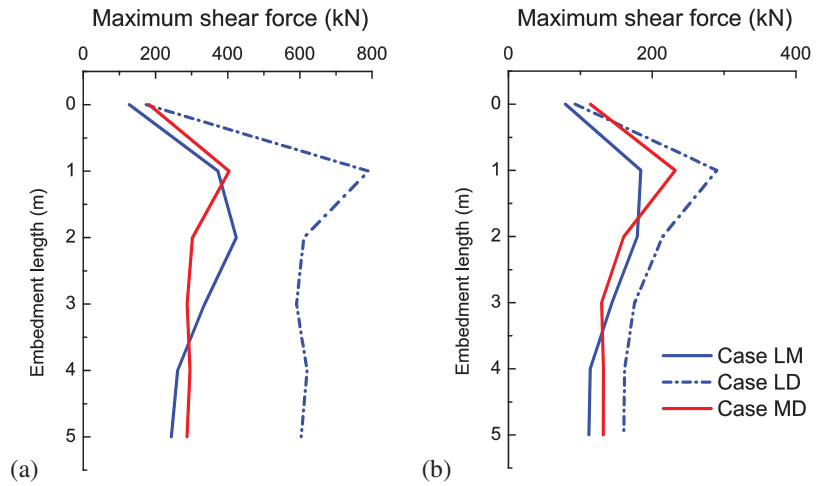

Figure 23. Maximum shear force along pile versus pile-embedment length under: (a) the Loma Prieta motion and (b) the El Centro motion.

5. Discussions and Conclusions

In this study, nonlinear dynamic interaction of piles and liquefiable ground is investigated using the open-source computational platform OpenseesPL. The dynamic behavior of the liquefiable soils is modeled by an extensively validated soil constitutive model based on the multi-surface-plasticity theory for frictional sandy soils. Efforts have been made to explore the effectiveness of the pile reinforcement to reduce lateral displacement in liquefied soils. In this investigation, parametric study was conducted by varying the area replacement ratio and pile-embedment length. Specifically, two-layer soil profiles were designed in numerical simulations (Case LM, Case LD, and Case MD).

The numerical simulations provide detailed analyses of progressive development of excess pore water pressure, stress, and strain in the soil–pile system. In general, installation of reinforcement piles does not prevent soils from liquefaction due to the fact that liquefaction initiation occurs at a relatively small strain level. However, pile installation can potentially reduce large flow deformation in the liquefied ground.

It has been found that embedding piles into a denser soil medium is important to ensure the effectiveness of mitigating lateral displacement in liquefied ground using reinforcement piles. The embedment length is an important consideration when there is no rigid rock founded to support the pile base. Assuming a fixed-end pile condition would result in the estimated ground displacement to be the smallest (unconservative), but the internal load in the pile to be largest (overly conservative), when compared with other embedment conditions. On the other hand, if the pile is not embedded into a denser layer, a large lateral displacement similar to the free field case would be observed, showing that pile installation has virtually no mitigating effect.

It should be noted that the total reduction of ground lateral displacement through increasing embedment length is limited by a critical value due to the nature of underlying soils, that is, further increase in embedment length may not result in effective reduction of displacement after a critical embedment length is reached. Specifically, if the underlying

soil is a dense sand (i.e., computational Cases LD, MD), an embedment length of at least 1 m is recommended. If the underlying soil is a medium sand (i.e., computational Case LM), larger embedment length (greater than 2 m) is required since the medium soil layer provides less competent support to the piles, and the soil layer may also be liquefied. For the case LM, the maximum lateral displacement can be large even with reinforcement piles installed (e.g., reaching 1 m under the El Centro motion), showing that the mitigation effect is limited in this condition, and the lateral displacement cannot be reduced to a satisfactory level by solely increasing the embedment length if the underlying soil is not strong enough. In such cases, it is highly recommended to assess the lateral displacement and internal stress/moment in piles using advanced computational tools, such as the OpenseesPL adopted throughout the study.

In terms of internal forces, case LD has the highest internal shear and bending moment along the pile. This is due to a larger difference in density between the upper and lower layer of soils. Furthermore, it has been founded that the Loma Prieta motion, which has less number of significant cycles but higher energy flux, creates higher internal forces to all computational cases. It is also worth mentioning that the Loma Prieta motion has a higher maximum loading on the pile than the El Centro motion, indicating that ground-motion characteristics is definitely influential to the effectiveness of ground improvement.

Note that numerical studies in this paper may have many limitations pertinent to modeling of post-liquefaction soil behavior. Recent centrifuge tests reported that the post-liquefaction flow can be in the order of meter even though the site was mitigated using fixed-end piles [Takahashi *et al.*, 2016]. More case histories and experimental studies are greatly needed to validate the numerical simulations and provide more insights into this topic.

Funding

This work was supported by the Hong Kong Research Grants Council [Grant Nos. 16213615, T22-603/15N] and the National Natural Science Foundation of China [Grant No. 51639006], which are greatfully acknowledged.

References

Adalier, K. and Elgamal, A. [2004] "Mitigation of liquefaction and associated ground deformations by stone columns," *Engineering Geology* **72**, 275–291.

Arulmoli, P. E., Martin, G. R., Gasparro, M. G., Shahrestani, S. and Buzzoni, G. [27–31 July 2004] "Design of pile foundations for liquefaction-induced lateral spread displacements," *GeoTrans*, Los Angeles, CA.

Asgari, A., Oliaei, M. and Bagheri, M. [2013] "Numerical simulation of improvement of a liquefiable soil layer using stone column and pile-pinning techniques," *Soil Dynamics and Earthquake Engineering* **51**, 77–79.

Berrill, J. and Yasuda, S. [2002] "Liquefaction and piled foundations: some issues," *Journal of Earthquake Engineering* **6**(S1), 1–41.

Boulanger, R. W., Chang, D., Gulerce, U., Brandenberg, S. J. and Kutter, B. L. [2006] "Evaluating pile pinning effects on abutments over liquefied ground," Workshop on seismic performance and simulation of pile foundations in liquefied and laterally spreading ground," *Geotechnical Special Publications GSP* **145**, 306–318.

Du, W. and Wang, G. [2017] "Empirical correlation between the effective number of cycles and other ground motion intensity measures," *Soil Dynamics and Earthquake Engineering* **102**, 65–74.

Elgamal, A., Lu, J. and Forcellini, D. [2009] "Mitigation of liquefaction-induced lateral deformation in a sloping stratum: 3D numerical simulation," *Journal of Geotechnical and Geoenvironmental Engineering* **135**(11), 1672–1682.

Elgamal, A., Yang, Z., Parra, E. and Ragheb, A. [2003] "Modeling of cyclic mobility in saturated cohesionless soils," *International Journal of Plasticity* **19**, 883–905.

Idriss, I. M. and Boulanger, R. W. [2008] "Soil Liquefaction during Earthquake," EERI Publication, Monograph MNO-12, Earthquake Engineering Research Institute, Oakland.

Ishihara, K. [1993] "Liquefaction and flow failure during earthquakes," *(Rankine Lecture) Géotechnique* **43**, 351–415.

Lew, M., Shao, L., Hudson, M. B. and Murphy, M. A. [2014] "Mitigation of soil liquefaction by deep soil mixing for hospitals," *Proceedings of the 10th National Conference in Earthquake Engineering*, Earthquake Engineering Research Institute, Anchorage, AK.

Lu, J., Elgamal, A., Yan, L., Law, K. H. and Conte, J. P. [2011b] "Large-scale numerical modeling in geotechnical earthquake engineering," *International Journal of Geomechanics*, 490–503. doi:10.1061/(ASCE)GM.1943-5622.0000042.

Lu, J., Elgamal, A. and Yang, Z. [2011a] "OpenSeesPL: 3D lateral pile–ground interaction user manual (Beta 1.0)," Dept. of Structural Engineering, Univ. of California, San Diego.

Maheshwari, B. K. and Sarkar, R. [2011] "Seismic behavior of soil–pile-structure interaction in liquefiable soils: parametric study," *International Journal of Geomechanics*, 335–347. doi:10.1061/(ASCE)GM.1943-5622.0000087.

Nguyen, T. V., Rayamajhi, D., Boulanger, R. W., Ashford, S. A., Lu, J., Elgamal, A. and Shao, L. [2013] "Design of DSM grids for liquefaction remediation," *Journal of Geotechnical and Geoenvironmental Engineering*, 1923–1933. doi:10.1061/(ASCE)GT.1943-5606.0000921.

Phanikanth, V. S., Choudhury, D. and Reddy, G. R. [2013] "Behavior of single pile in liquefied deposits during earthquakes," *International Journal of Geomechanics*, 454–462. doi:10.1061/(ASCE)GM.1943-5622.0000224.

Rayamajhi, D., Nguyen, T. V., Ashford, S. A., Boulanger, R. W., Lu, J., Elgamal, A. and Shao, L. [2014] "Numerical study of shear stress distribution for discrete columns in liquefiable soils," *Journal of Geotechnical and Geoenvironmental Engineering*, 04013034. doi:10.1061/(ASCE)GT.1943-5606.0000970.

Takahashi, H., Takahashi, N., Morikawa, Y., Towhata, I. and Takano, D. [2016] "Efficacy of pile-type improvement against lateral flow of liquefied ground," *Géotechnique* **66**(8), 617–626.

Tokimatsu, K. and Nomura, S. [1991] "Effects of ground deformation on piles stresses during soil liquefaction," *Journal of Structural and Construction Engineering* **426**, 107–113 (in Japanese).

Wang, G. and Sitar, N. [2011] "Static and dynamic axial response of drilled piers. II: Numerical evaluation," *Journal of Geotechnical and Geoenvironmental Engineering* **137**(12), 1143–1153.

Wang, G. and Wei, J. [2016] "Microstructure evolution of granular soils in cyclic mobility and post-liquefaction process," *Granular Matter* **18**, 51.

Wei, J., Huang, D. and Wang, G. [2018] "*Micro-Scale Descriptors for Particle-Void Distribution and Jamming Transition in Pre- and Post-Liquefaction of Granular Soils*," Journal of Engineering Mechanics ASCE (in press).

Xie, Y. and Wang, G. [2014] "A stabilized iterative scheme for coupled hydro-mechanical systems using reproducing kernel particle method," *International Journal for Numerical Methods in Engineering* **99**(11), 819–843.

Yang, Z., Elgamal, A. and Parra, E. [2003] "Computational model for cyclic mobility and associated shear deformation," *Journal of Geotechnical and Geoenvironmental Engineering* **129**(12), 1119–1127.

Ye, J. H., Huang, D. and Wang, G. [2016] "Nonlinear simulation of offshore breakwater on sloping liquefied seabed," *Bulletin of Engineering Geology and the Environment* **75**, 1215–1225.

Ye, J. H. and Wang, G. [2015] "Seismic dynamics of offshore breakwater on liquefiable seabed foundation," *Soil Dynamics and Earthquake Engineering* **76**, 86–99.

Ye, J. H. and Wang, G. [2016] "Numerical simulation of the seismic liquefaction mechanism in an offshore loosely deposited seabed," *Bulletin of Engineering Geology and the Environment* **75**, 1183–1197.

Zhang, G. and Wang, L. [2010] "Stability analysis of strain-softening slope reinforced with stabilizing piles," *Journal of Geotechnical and Geoenvironmental Engineering* **136**(11), 1578–1582.

Zienkiewicz, O. C., Chan, A. H. C., Pastor, M., Paul, D. K. and Shiomi, T. [1990] "Static and dynamic behavior of soils: a rational approach to quantitative solutions: I. Fully saturated problems," *Proceedings of the Royal Society of London: Series A* **429**, 285–309.